Aquaculture 591 (2024) 741140

Contents lists available at ScienceDirect

Aquaculture

journal homepage: www.elsevier.com/locate/aquaculture

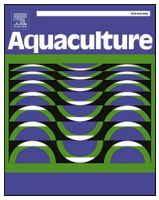

Understanding morphological rib abnormalities in Atlantic salmon

Raúl Jiménez-Guerrero [a,*], Grete Baeverfjord [b], Øystein Evensen [c], Turid Mørkøre [a]

[a] Department of Animal and Aquacultural Sciences, Faculty of Biosciences, Norwegian University of Life Sciences, NO-1432 Ås, Norway
[b] Nofima, NO-6600, Sunndalsøra, Norway
[c] Department of Paraclinical Sciences, Faculty of Veterinary Medicine, Norwegian University of Life Sciences, NO-1433 Ås, Norway

ARTICLE INFO

Keywords:
Rib malformation
Rib degeneration
Osteomalacia
Farmed fish
Fish welfare

ABSTRACT

Poor rib health in Atlantic salmon (*Salmo salar* L.) can lead to negative effects on welfare and fillet quality. The present research aimed to enhance the comprehension of long-term rib morphology within a broader musculoskeletal framework of harvest-sized salmon (3 kg), examining a population fed different smoltification diets. Generally, X-ray examinations revealed the highest concentration of abnormalities in the anterior-central area of the rib cage, and the mid-distal rib parts. The different diets, based on either marine (M-group) or vegetal (V-group) ingredients, modulated the morphology of the ribs in the central area of the rib cage. Compared to the V-group, the M-group had a lower prevalence of generalized radiolucency (GR) (19 vs. 26% of mid-distal rib parts), and axis deformations/malformations (12 vs. 17% of mid rib parts). Histological examination of GR, unrelated to near inflammatory processes, revealed potential degradation/transformation of central core chondrocytes to mesenchymal-like cells. The newly formed cavity progressed/expanded through osteolysis until it reached the periosteum. In parallel, there were progressive alterations of the concentric appositional growth pattern of the compact bone, with an increase of the external collagen layer under the cellular periosteum. Disorganized collagen-rich islands were also seen in the compact bone, as were signs of new osteoid deposition in the cavity. The degenerative process in GR was accompanied by an 18–20% increase in the cross-sectional diameter of the rib. The M-group presented numerically higher mechanical rib strength ($p = 0.06$), and phosphorus content ($p = 0.07$). The sensitivity of rib morphology to smoltification diet was higher than vertebrae in the long-term. This study enhances understanding of the etiology of the primary morphological rib abnormalities in Atlantic salmon, particularly in GR, by providing detailed histomorphology of pathological changes. The study associates these changes with altered rib development, degeneration, and possibly osteomalacia.

1. Introduction

Understanding the skeletal health of Atlantic salmon (*Salmo salar* L.), is of critical importance, as it is essential for the shape and protection of soft tissues, structure support, and swimming (Gray, 1957; Kryvi and Poppe, 2016). Poor skeleton health directly impacts fish welfare (Noble et al., 2018), but also business profitability as it negatively affects fish growth (Hansen et al., 2010), product and technological quality of fillets (Currey, 2003; Haugarvoll et al., 2010; Sullivan et al., 2007). Currently, salmon bone research is focused on vertebral health (Drábiková et al., 2021, 2022; Witten et al., 2019), while there has been much less focus on the rib cage. Rib (*pleurapophysis*) morphology, mechanical properties and chemical composition of cellular and acellular bone have already been studied in several fish species (Cohen et al., 2012; De Clercq et al., 2017; Horton and Summers, 2009; Jiao et al., 2020; Soliman, 2018). Although rib malformations have been described in zebrafish (*Danio rerio*) (Akama et al., 2020), and rainbow trout (*Oncorhynchus mykiss*) (Gislason et al., 2010), to our knowledge, only a few studies focus on Atlantic salmon.

Recently, Jiménez-Guerrero et al. (2022) and later Brimsholm et al. (2023) used X-ray and histology to explore rib morphology and its relationship with red (acute; hemorrhages) and black (chronic) focal dark spots (DS) of fillets, the largest fillet quality concern of farmed salmon (Nordberg, 2018). They described the presence of deviations along the proximo-distal axis (axis deviations), changes in radiodensity, and fractures in farmed and wild salmon. Jiménez-Guerrero et al. (2022) reported occurrence of eight different types of morphological rib abnormalities in the rib cage, where the number of axis deviations, generalized radiolucency (dark X-ray appearance indicating lower mineral density), shorter or missing rib parts, radiolucent and

* Corresponding author.
E-mail address: raul.jimenez.guerrero@nmbu.no (R. Jiménez-Guerrero).

https://doi.org/10.1016/j.aquaculture.2024.741140
Received 5 September 2023; Received in revised form 18 May 2024; Accepted 23 May 2024
Available online 24 May 2024
0044-8486/© 2024 The Authors. Published by Elsevier B.V. This is an open access article under the CC BY license (http://creativecommons.org/licenses/by/4.0/).

radiopaque (light X-ray appearance indicating high mineral density) calluses may depend on the life stage and growing environment. The transition from fresh- to seawater appeared to be critical, causing increasing generalized radiolucency and shorter or missing ribs. Among different etiological factors, traumatic events causing rib cage deformation/damage, local inflammatory processes, and time-specific dietary deficiencies were suggested.

Skeletal malformations usually develop during early life stages (Baeverfjord et al., 2018; Fjelldal et al., 2009; Vielma and Lall, 1998). Though Brimsholm et al. (2023) suggested that generalized radiolucency and axis deviations in ribs are a normal morphological variation, Baeverfjord et al. (1998) previously reported axis deviations in the form of malformed wrinkly ribs (irregularity in surface contour marked by folds, creases, and ridges) and mechanical deterioration in response to a phosphorus (P) deficient diet during fresh and seawater phases. Later, Roberts et al. (2001) observed similar findings associated with dietary P and vitamin C deficiency during early life stages. While many of these studies are primarily descriptive, our understanding of salmon rib health remains nascent. Hence, the present study aimed to improve the understanding of rib abnormalities of adult Atlantic salmon and to reveal whether abnormal rib morphology is influenced by smoltification feeding.

2. Material and methods

2.1. Fish material

Atlantic salmon eggs of common genetic origin (BO 1–20, AS Bolaks, Eikelandsosen, Bjørnafjorden, Norway) were hatched at the Research Station for Sustainable Aquaculture (Nofima, Sunndalsøra, Møre and Romsdal, Norway) December 6th 2019. On July 7th 2020 1600 fish averaging 30 g were PIT-tagged and fed either a marine-based diet (M-group) or a vegetal-based diet (V-group) in quadruplicate tanks per dietary treatment ($n = 200$ per tank; flow-through; tank volume, 0.5 m^3) (Supplementary 1, Supplementary 2, and Supplementary 3). Smoltification was induced following a 12:12 Light:Dark hours regime from July 13th 2020. On August 26 – 27th 2020, all fish were vaccinated with Alpha JECT® micro 6 by hand injection (PHARMAQ AS, Overhalla, Norway). Smoltification status was checked by challenge test, plasma osmolality determination, chloride content, and gill Na^+, K^+-ATPase activity on September 4th, 11th, and 15th 2020 ($n = 12$, 12, and 12) (Clarke et al., 1996). On September 16th 2020, 25 fish from each tank ($n = 100$ per dietary treatment) were mixed and randomly transferred to two seawater tanks (flow-through; 3 m^3). Fish were fed a standard commercial diet with pellet size and composition adjusted to fish size according to feed producer recommendations (Skretting, Stavanger, Norway) during the entire seawater phase. The light regime was continuous, tank biomass was kept under 30 kg/m^3 by splitting the fish into two to three (February 12th 2020) and four (June 1st 2020) tanks, and water flow was 100 l/min. On 22nd July 2021, 168 fish ($n = 84$ per dietary group; $n = 21$ per original quadruplicate tank; 2.6 kg average body weight) were carefully transferred to a large common tank (flow-through; 103 m^3), where experience from the research station has shown that DS can develop. The water flow gradually increased from 700 to 1200 l/min, and the light regime was kept continuous. On September 16th – 17th 2021 (3 kg average body weight), the experiment was terminated. More details about the experiment can be found in Supplementary 4 and Supplementary 5.

2.2. Diets

The test diets were produced by extrusion at the Aquafeed Technology Centre (Nofima, Bergen, Norway). Diets were qualitatively different, isoenergetic, and of similar pellet size (2 mm). While the M-group diet was formulated with exclusively fish meal and oil, and wheat starch (binder), the V-group diet was formulated using soy protein concentrate, wheat gluten, corn gluten, and rapeseed oil. The raw formulation and composition of the M- and V-group diets are presented in Supplementary 1, Supplementary 2, and Supplementary 3. Pellet properties are described in Karki (2022).

Test and standard feed samples were homogenized and analyzed for protein (ISO5983-2, 2009), fat (EC152, 2009), dry matter (ISO6496, 1999), ash content (ISO5984, 2002), fiber (AOCSBa6a-05, 2017), combustion value (energy) (ISO9831, 1998), total starch and free astaxanthin (BioLab internal protocol, Nofima, Bergen, Norway), and amino acid composition (ISO13903, 2005). The fatty acid composition was determined by gas chromatography (GC) as fatty acids methyl esters using 23:0 as the internal standard. The concentrations of calcium (Ca), P, magnesium (Mg), potassium (K), sodium (Na), zinc (Zn), iron (Fe), manganese (Mn), and copper (Cu) were determined spectrophotometrically after digestion with acid using an MP-AES (Microwave Plasma Atomic Emission Spectrometer) (Agilent Technologies, Santa Clara, California, USA). Soluble P was indirectly estimated by the colorimetric detection (880 nm absorption) of ascorbic acid-molybdate phosphate on a spectrophotometer (Shimadzu UVmini 1210, Shimadzu Europe, Duisburg, Germany) (ISO6878, 2004).

2.3. Sampling

Fish were sampled three times during the experimental period; September 16th 2020 (prior to seawater transfer), December 3rd 2020 (10 weeks after seawater transfer), and September 16th – 17th 2021 (harvest). Fish for analyses after seawater transfer were sampled representing the original dietary tanks in freshwater based on PIT-tags readings. At sampling, fish were euthanized by an overdose of MS-222 (Metacaine 0.1 g l − 1; Alpharma, Animal Health Ltd., Hampshire, UK) before blood was collected from the caudal vein. Thereafter, fish were bled out by the gill section, and individual weight and length were recorded. On September 16th 2020, randomly selected fish were sampled from three tanks per dietary treatment ($n = 15$ per dietary group). All fish were sampled for blood, gutted and kept at −20 °C for X-ray and mineral analyses. On December 3rd 2020 ($n = 50$ per dietary group), blood samples were taken from 10 fish per dietary group. The presence of DS was recorded ($n = 40$ per dietary group). A group of gutted fish ($n = 10$ per dietary group) was kept at −20 °C for X-ray analyses. On September 16th – 17th 2021, at harvest ($n = 80$ per dietary group), blood samples were taken from 12 fish per dietary group. The abdominal right-side wall (parietal peritoneum, rib, and adjacent skeletal muscle) corresponding to rib numbers 11 to 14 at the mid position (median region between proximal rib head and distal tip) of the ribs was sampled for histomorphology examinations of 12 fish per dietary group. These samples and DS (red, n = 4; black, $n = 3$) were fixed in formalin (10% phosphate-buffered formalin, pH 7.0, 4 °C). Twenty fish per dietary treatment were filleted pre-rigor and transported in styrofoam boxes with ice to Nofima Ås laboratory for fillet quality analysis (color, firmness, gaping, and DS) after five days, whereas a group of 40 gutted fish per dietary group was kept at −20 °C for X-ray, mechanical properties and mineral analyses of ribs and vertebrae. Strength and mineral analyses of the rib cage ($n = 12$ per dietary group) and vertebrae ($n = 20$ per dietary group) were performed using selected fish with no vertebrae abnormalities.

2.4. X-ray

X-rays of frozen fish and formalin-fixed material were performed at the Nofima radiography laboratory in Sunndalsøra. Samples of fish prior to and after seawater transfer, the right and left sides of the rib cage of fish at harvest, and targeted formalin-fixed samples of fish at harvest were X-rayed using an IMS Giotto mammography equipment (Giotto, Pontecchio Marconi, BO, Italy), with 20 pixels per mm^2 resolution, exposure at 22 kV and 100 mAs. For gutted fish sampled at harvest, X-rays were taken using a semi-digital computed radiography system (Fuji

Medical AS, Oslo, Norway). Prior to rib cage X-rays, frozen gutted bodies were thawed at 4 °C for three days. Rib cages were cut and trimmed at room temperature. Images were taken on coated photo-reactive phosphorous imaging plates Fujifilm Computed Radiography (FCR) (Fujifilm, Tokyo, Japan), and read using FCR Profect Reader (Fujifilm, Tokyo, Japan). Sample preparation and evaluation of rib morphology at proximal, mid and distal parts, as well as at the anterior (ribs 1–7), central (ribs 8–15) and posterior (ribs 16–22) areas of the rib cage were performed according to Jiménez-Guerrero et al. (2022). Evaluation of vertebral morphology was done similarly to Bou et al. (2017) and Fjelldal et al. (2007). However, major morphological abnormalities like compression, fusion, and cross-stitch were distinguished from deviations in vertebra width or length (X) versus height (Y) (X:Y ratio) (Bou et al., 2017), and internal structural malformation of the vertebral body (Witten et al., 2019). The impaired mineralization score was performed according to the scale in Supplementary 6. After X-ray analyses, fish sampled prior to seawater transfer were pooled per original freshwater tank based on the PIT-tag numbers and stored at −20 °C for mineral analyses. Rib cage skeletons and vertebrae from vertebra number 31 to 41 of harvest fish were kept at 4 °C for mechanical analysis. Formalin-fixed material was stored at 4 °C.

2.5. Histology

Formalin-fixed samples were decalcified (EDTA 10%; pH 7) at room temperature for two weeks, before they were dehydrated, embedded in paraffin wax, and sectioned at 2–2.5 μm. Sections of the abdominal wall were performed horizontally at the center of the sample to obtain a cross-sectional view of 3–4 ribs and adjacent tissues (Supplementary 7). DS were sectioned parallel to the parietal peritoneum. Sections were mounted on glass slides, stained with Haematoxylin and Eosin, Periodic acid–Schiff, Movat Pentachrome, and Picro Sirius Red, scanned using NanoZoomer S360 (C13220–01, Hamamatsu Photonics K·K, Hamamatsu, Japan), and visualized with NDP.view.2 (v.2.7.43, Hamamatsu Photonics K·K, Hamamatsu, Japan). Picro Sirius Red-stained sections were inspected under polarized light by a Leica DM6B Light microscope with a DMC4500 Digital Camera (Leica Microsystems, Wetzlar, Germany) at 90° (cross polarization), and for confocal microscopy with a Leica TCS SP5 Confocal laser scanning microscope (Leica Microsystems, Wetzlar, Germany) using two channels (emission bandwidth, 496 nm – 554 nm and 574 nm – 644 nm).

The morphometry of the ribs was evaluated using the transverse fascia as a reference point. The parallel line, representing the combined thickness of the rib bone, periosteum, and adjacent fat (referred to as the rib cluster), was collected at the rib's center (Supplementary 7). The cross-sectional micro-organization of the compact bone from normal ($n = 4$) and abnormal ribs ($n = 6$) was studied by gray level co-occurrence matrix texture analysis, using the ImageJ software (v1.52s, U. S. National Institutes of Health, Bethesda, USA), plug-in "GLCM Texture" on Picro Sirius Red-stained images. Prior to grayscale transformation (8-bit images), images from individual ribs and adjacent soft tissues were generated, and histogram equalized. Then, compact bone was manually selected (Supplementary 8) to perform the gray level co-occurrence matrix texture analysis with the size of the step-in pixels set to 1 using 0 and 90° directions. The following parameters were extracted (Zaletel et al., 2017): angular second moment and inverse difference moment as measures of image homogeneity; and contrast and entropy as a measure of heterogeneity. Values for 0 and 90° direction were averaged because the aleatory position of ribs made it impossible to study linear dependencies.

Osteocyte density was calculated by dividing the number of local maxima corresponding to osteocytes or lacunae in compact bone ("Find Maxima" function; prominence >25; excluding edges maxima; light background) by the selected area (μm^2) (Supplementary 8).

2.6. Bone dissection, strength measurement, and mineral content

Rib numbers 1–22 from rib cages sampled at harvest were dissected from the fish peritoneum using metal pincers, and the remaining attached flesh was carefully removed. Ribs number 12, 13, and 14 from the left and right sides were selected for mechanical analyses. Prior to the mechanical test, ribs were kept for two hours on a dry surface at room temperature to standardize moisture levels. Mechanical analyses were performed instrumentally (TA-XT2 Texture Analyzer, Stable Micro Systems, Surrey, UK), with a guillotine knife (70 mm width, 3 mm thickness) and well bottom surface at three different rib parts: proximal, mid, and distal (Jiménez-Guerrero et al., 2022). The trigger force was 1 Newton at a traveling speed of 2 mm/s. Strength values were recorded as breaking load (N) and the elasticity (slope) at 50% of the breaking load. Following the test, all ribs were pooled per original freshwater tank based on the PIT-tag numbers and stored at −20 °C for mineral analysis.

Vertebrae were dissected and trimmed to minimize the contact between the knife and those parts not belonging to the vertebral body. Two separated vertebrae from each fish were latero-laterally compressed to emphasize the trabecular fraction as it is naturally more active than the compact bone (Gil Martens et al., 2006; Nordvik et al., 2005). Analyses were performed using the same instruments and guillotine knife as ribs but with a trigger load of 10 Newton at a traveling speed of 2 mm/s. Strength values were collected from the given time-load graphs as load (N), elasticity (slope), and area as work (N*mm) at 50% of the compression depths due to the structural symmetry of the vertebra body. Values from both vertebral measurements per fish were averaged. After the test, vertebrae were pooled per original freshwater tank based on the PIT-tag numbers ($n = 4$ per dietary treatment) and stored at −20 °C for mineral analysis.

Ribs and vertebrae from harvest fish were homogenized. Fish bodies sampled prior to seawater transfer were gutted and homogenized. Excluding ribs, homogenized samples were heated for dry matter (ISO6496, 1999) and ash content (ISO5984, 2002) determination. The concentrations of Ca, P, Mg, K, Na, Zn, Fe, Mn, and Cu were determined spectrophotometrically after digestion with acid using an MP-AES. Due to the low volume of pooled homogenized ribs, only total Ca, P, and Mg were analyzed. Ca and Mg concentration was assessed using inductively coupled plasma mass spectrometry (ICP-OES) after microwaved digestion. Total P concentration was estimated through an individual spectrophotometrically method (ISO6491, 1998).

2.7. Macroscopic muscle straits

Fillet color was assessed using DSM SalmoFan™ (F. Hoffmann-La Roche AG, Basel, Switzerland), and the severity of gaping was assessed by the average gaping score (from 0, no gaping, to 5, severe gaping) (Andersen et al., 1994) of the left and right fillets. The mechanical properties of fillets were determined as the firmness at the dorsal loin (epaxial skeletal muscle) of the right fillet as the force required to break the fillet surface (breaking force, N) using the same instruments as for bone, but with a flat-ended 12.5 mm probe at a traveling speed of 1 mm/s (Mørkøre and Einen, 2003). The presence of DS was evaluated according to their size and color using a log-2 scoring system from 0 (no visible DS) to 8 (DS > 6 cm width) (Mørkøre, 2012).

2.8. Serum chemistry

Blood was extracted using 6 ml vacutainer tubes and centrifuged at 3700 RPM at ambient temperature for 10 min, using an Avanti J-15R centrifuge (Beckman Coulter, Inc., Indianapolis, United States) with a radius rotor of 207.8 mm for serum extraction. Serum was pooled in groups of five fish per original freshwater tank and stored at −20 °C for clinical biochemistry analysis (Faculty of Veterinary Medicine, NMBU, Norway). Due to the high dietary differences, the concentration of several standard health parameters in serum was explored to monitor

Table 1
Morphology, mechanical properties, and mineral composition of ribs of Atlantic salmon at harvest (3 kg). The fish were fed either a marine-based diet (M-group) or a plant-based diet (V-group) during smoltification.

Rib parameters		M-group	V-group	*p* value
Longitudinal morphology (number of rib abnormalities)				
Category I (no continuity break)		6 ± 0.9	11.5 ± 1.2	< 0.001
	Generalized radiolucent	1.9 ± 0.4	5.0 ± 1	< 0.001
	Axis deviations	4.0 ± 0.9	6.6 ± 1	0.01
Category II (continuity break)		3.0 ± 0.7	3.7 ± 0.4	0.36
	Fracture	0 ± 0	0.1 ± 0.1	1.00
	Supernumerary	0 ± 0	0 ± 0	1.00
	Radiolucent callus	0.8 ± 0.2	0.7 ± 0.2	0.86
	Radiopaque callus or hyperostosis	0.3 ± 0.2	0.2 ± 0.2	0.75
	Radiolucent non-union	0.1 ± 0.1	0 ± 0	0.65
	Shorter or missing parts	1.8 ± 0.5	2.7 ± 0.3	0.18
Total		9.0 ± 1.3	15.3 ± 1.4	< 0.001
	Proximal	0.5 ± 0.2	0.7 ± 0.2	0.52
	Mid	1.0 ± 0.5	5.0 ± 0.7	< 0.001
	Distal	7.4 ± 0.9	9.5 ± 0.9	0.08
Cross-sectional morphology (mm)				
Bone diameter		0.5 ± 0.03	0.5 ± 0.04	0.92
Periosteum width		0.2 ± 0.03	0.2 ± 0.01	0.74
Rib hub diameter		2.1 ± 0.22	2.0 ± 0.14	0.80
Mechanical properties				
Breaking load (N)				
	Proximal	10.8 ± 0.7	10.4 ± 0.6	0.65
	Mid	7.1 ± 0.4	7.0 ± 0.3	0.87
	Distal	5.5 ± 0.3	5.3 ± 0.2	0.70
Modulus of Elasticity (N mm^{-1})				
	Proximal	39.4 ± 2.5	36.8 ± 1.9	0.43
	Mid	30.6 ± 1.5	26.7 ± 1.4	0.06
	Distal	32.5 ± 3.1	28.9 ± 1.2	0.27
Mineral composition (ww)				
Ca (g kg^{-1})		137.5 ± 4.8	127.6 ± 2.5	0.11
P (g kg^{-1})		63.8 ± 2.9	55.3 ± 2.7	0.07
Ca:P ratio		2.2 ± 0.2	2.3 ± 0.1	0.51
Mg (g kg^{-1})		2.8 ± 0.3	3.0 ± 0.1	0.65

The longitudinal morphology is described as the number of rib abnormalities per rib cage side (22 ribs). Significant differences between groups were set to $p \leq 0.05$. Data are presented as non-transformed mean ± SEM, n = 12 (morphology), 20 (mechanical properties), and 4 (mineral composition; pooled per tank) per dietary group. N, Newton; ww, Wet weight; Ca, Calcium; P, Phosphorus; Mg, Magnesium.

different fish health indicators: alkaline phosphatase (ALP), a specific bone formation marker (Kuo and Chen, 2017); creatine kinase (CK) as a marker for disruption of cell membranes due to hypoxia or injury (Baird et al., 2012); creatinine as muscle development indicator (Patel et al., 2013); inorganic phosphorous (P*i*), calcium (Ca^{2+}), sodium (Na^{+}), and potassium (K^{+}) for available ions and electrolyte balance. Samples were analyzed using Atellica® CH (Siemens Healthcare Diagnostics Inc., Deerfield Road Deerfield, United States).

2.9. Statistics

Comparative tests were conducted between the V-groups and M-groups. The statistical analyses were performed with R software (v. 4.0.3, R Core Team, Vienna, Austria). For parametric traits, analyses were conducted using a linear model ("lm" R function), whereas for non-parametric traits, a generalized linear model ("glm" R function) was employed adjusted for either Poisson or binomial distributions. Pairwise test of non-parametric distributions between both dietary groups at different areas of the rib cage was performed using the Wilcoxon rank sum test ("pairwise.wilcox.test" R function, p.adjust.method = "BH"). The models did not consider random effects. Microsoft® Excel® software (v. 15,128.20280, Microsoft Corporation, Redmond, United States) was used to create figures. The significance level was set at $p \leq 0.05$, and results were presented as mean ± standard error (SEM).

3. Results

3.1. X-ray

At harvest, the number of rib abnormalities was found to increase from the proximal to distal rib parts. Rib abnormalities were mostly concentrated around rib number 9 for both dietary groups. However, the V-group showed 1.9 more abnormalities than the M-group in central ($p = 0.02$) and 5 times more abnormalities in mid areas ($p < 0.001$; Table 1) of the rib cage. These differences were contributed principally by two abnormality forms (Fig. 1). Firstly, axis deviations in the form of several parallel rib deformations in a linear pattern and particularly wrinkly malformations affecting 19% (M-group) and 26% (V-group) of studied ribs ($p = 0.01$; Table 1) in a decreasing number from anterior to posterior areas of the rib cage. Mid rib parts of the V-group presented more axis deviations than the M-group ($p < 0.001$). Secondly, generalized radiolucency affected 12% (M-group) and 17% (V-group) of studied ribs ($p < 0.001$), concentrated in central ($p = 0.061$) and mid-distal areas of the rib cage ($p < 0.001$) in the V-group, contrasting to the even distribution from rib number 1 to 22 in the M-group (Table 1).

Prior to seawater transfer, virtually no vertebral abnormalities nor

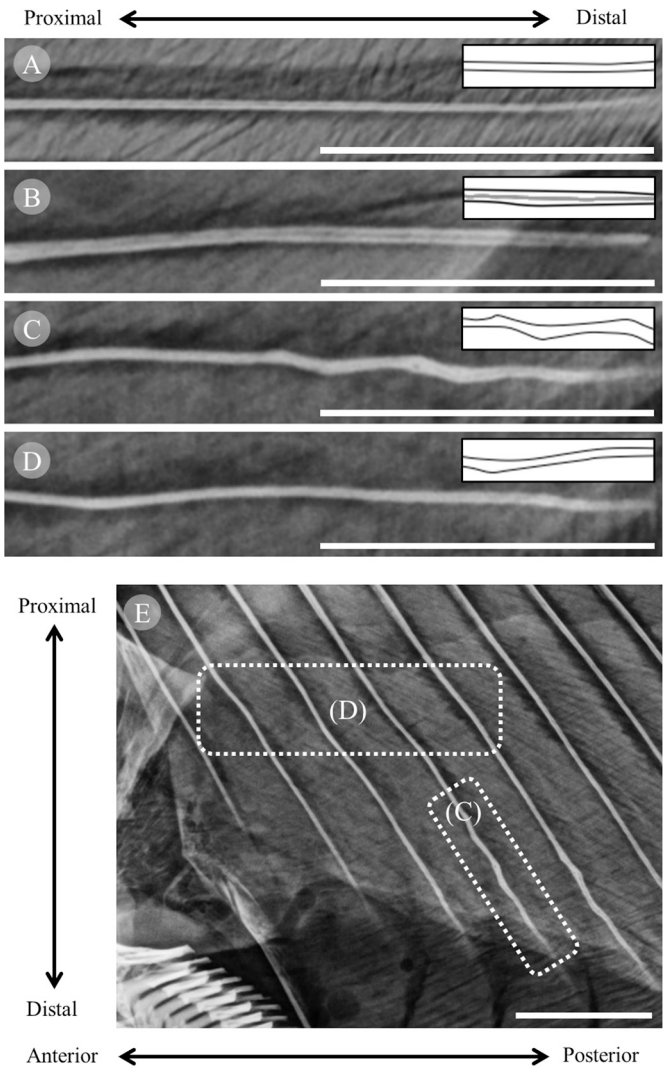

Fig. 1. Typical rib morphologies of Atlantic salmon (3 kg). Lateral X-ray. A) Normal rib, B) generalized radiolucency, C) wrinkly malformation, and D) deformation. A simplified illustration of the respective rib morphology from A) to D) is added in the top right corner. E) Rib cage side corresponding to rib numbers 1–8 with examples of axis deviations: D) parallel bent ribs in a linear pattern, and C) wrinkly morphology. The white bars on the bottom right corner show the image scale, set to 12 mm.

clinical morphological signs of impaired mineralization were observed. On the other hand, the vertebra X:Y ratio was lower in the V-group than in the M-group ($p = 0.01$). Ten weeks after seawater transfer, fish from both dietary treatments presented clear signs of impaired mineralization (likely P deficiency). However, the severity was more pronounced for the V-group, as indicated by a higher impaired mineralization score ($p = 0.049$) and a lower vertebra X:Y ratio ($p = 0.04$) (Table 2). Numerically lower vertebra X:Y ratio and more fused vertebrae were found in both groups than before seawater transfer. At harvest, the vertebra X:Y ratio increased to normal values, and no signs of residual dietary-induced internal malformations of the vertebral body were observed. The prevalence of fish from the M-group with abnormal vertebrae (17%) was not significantly different from the V-group (23%), nor was the magnitude (Supplementary 9). No differences were observed in the width of the intervertebral space between the dietary groups at any sampling time.

3.2. Rib histomorphology

Most (71%) rib cross-sections showed normal histological traits

Table 2
Biometric traits, fillet quality, and vertebrae morphology of Atlantic salmon assessed prior to seawater transfer, 10 weeks after transfer, and at harvest. The fish were fed either a marine-based diet (M-group) or a plant-based diet (V-group) during smoltification.

		Prior to seawater transfer				After seawater transfer				Harvest			
Parameters		M-group	V-group	*p* value	n	M-group	V-group	*p* value	n	M-group	V-group	*p* value	n
Biometric traits	Body weight (g)	111.7 ± 3.6	81.3 ± 2.9	< 0.001	15	281 ± 3.9	250.8 ± 5.9	0.003	40	3046 ± 68	3132 ± 71	0.24	80
	Condition factor	1.28 ± 0.03	1.29 ± 0.02	0.28	15	1.12 ± 0.01	1.15 ± 0.02	0.14	40	1.46 ± 0.01	1.48 ± 0.01	0.02	80
Fillet quality	Firmness (N)	.	.	.		.	.	.		11.8 ± 2.7	10.5 ± 2.4	0.049	20
	Gaping (score)	.	.	.		.	.	.		0.1 ± 0.1	0.4 ± 0.1	0.03	20
Vertebrae morphology	Abnormal vertebrae (%)	0	8	0.33	15	20	10	0.56	10	17	23	0.52	40
	Impaired mineralization score	0	0	.	15	0.76 ± 0.24	1.4 ± 0.19	0.049	10	0	0	.	20
	Vertebra X:Y ratio	0.96 ± 0.01	0.93 ± 0.01	0.01	15	0.93 ± 0.01	0.90 ± 0.01	0.04	10	1.03 ± 0.01	1.02 ± 0.01	0.39	20
	Intervertebral space (mm)	0.36 ± 0.01	0.34 ± 0.01	0.12	15	0.50 ± 0.03	0.50 ± 0.02	0.97	10	0.15 ± 0.03	0.16 ± 0.03	0.81	20

Significant differences between groups were set to $p \leq 0.05$. Data are presented as non-transformed mean ± SEM. Condition factor = 100*body weight/(body length)^3.

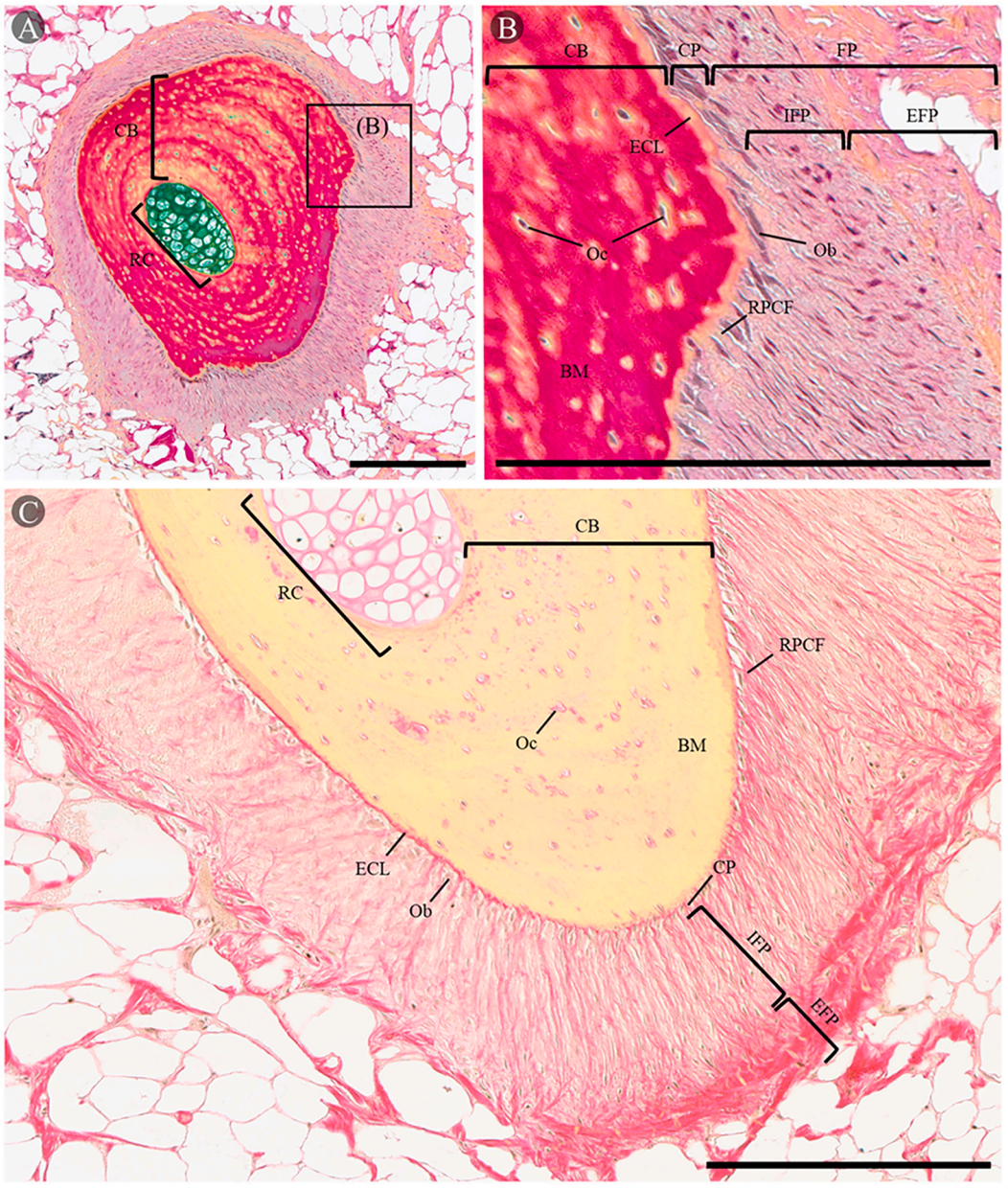

Fig. 2. Cross-sectional morphology of normal mid rib parts of Atlantic salmon (3 kg). For A) and B) Movat Pentachrome staining was used for proteoglycans and mucins (blue), collagen/reticular fibers (yellow), colocalization of collagen/reticular fibers and proteoglycans (green), muscle and osteoid (or decalcified bone matrix) (reddish-brown), nuclei and elastin (black) and active nucleus (osteoblast in cellular periosteum) (violet/purple). The box in image A) indicates the region of zoom of image B). Picro Sirius Red staining was used in C) to highlight the collagen fiber network (red) in the periosteum. CB, Compact bone; RC, Rib core with hyaline-cell (hypertrophic-like) cartilage; Oc, Osteocytes; BM, Bone matrix, ECL; External collagen layer of the CB; Ob, Osteoblast; CP, Cellular periosteum with Ob; FP, Fibrous periosteum; IFP, Internal fibrous periosteum; EFP, External fibrous periosteum; RPCF, Radial periosteal collagen/Sharpey's fibers. Black bars on the bottom right corner show the image scale, set to 250 μm. Color print. (For interpretation of the references to color in this figure legend, the reader is referred to the web version of this article.)

viewed by light microscopy, whereas a smaller proportion (29%) displayed noticeable deviations regardless of the dietary treatment before seawater transfer.

Normal ribs showed multiple concentric layers of osteocytes from the appositional growth of the compact bone. The radiopaque bone matrix presented collagen and non-collagen proteins organized around a hyaline-cell cartilage (hypertrophic-like) of relatively higher radiolucency. Perpendicular collagen fibers in the rib core showed a type III signal (Fig. 2. A; Fig. 3. A and C). Compact bone had a relatively lower amount of collagen fibers than the periosteum, where their perpendicular fibers were mainly type III (Fig. 2. C; Fig. 3. A and C). Osteocyte density was around 0.003 cells/μm^2. The rib periosteum presented an irregular thickness on the internal and external fibrous fractions. Radial glycoproteins and collagen type I and III fibers seemed to connect the fibrous periosteum to the outermost compact bone layer, occasionally forming a small shield with visible perpendicular collagen type I under the osteoblasts (Fig. 2. B and C; Fig. 3. C and E). Within the periosteum, the polarized signal near the compact bone and the external fibrous periosteum layer was stronger than in the center of the internal fibrous periosteum, suggesting that some fibers may run back (not perpendicular signal) into the bone (Sharpey's fibers) (Fig. 3. A). The external fibrous periosteum layer surrounding the ribs had the richest content of

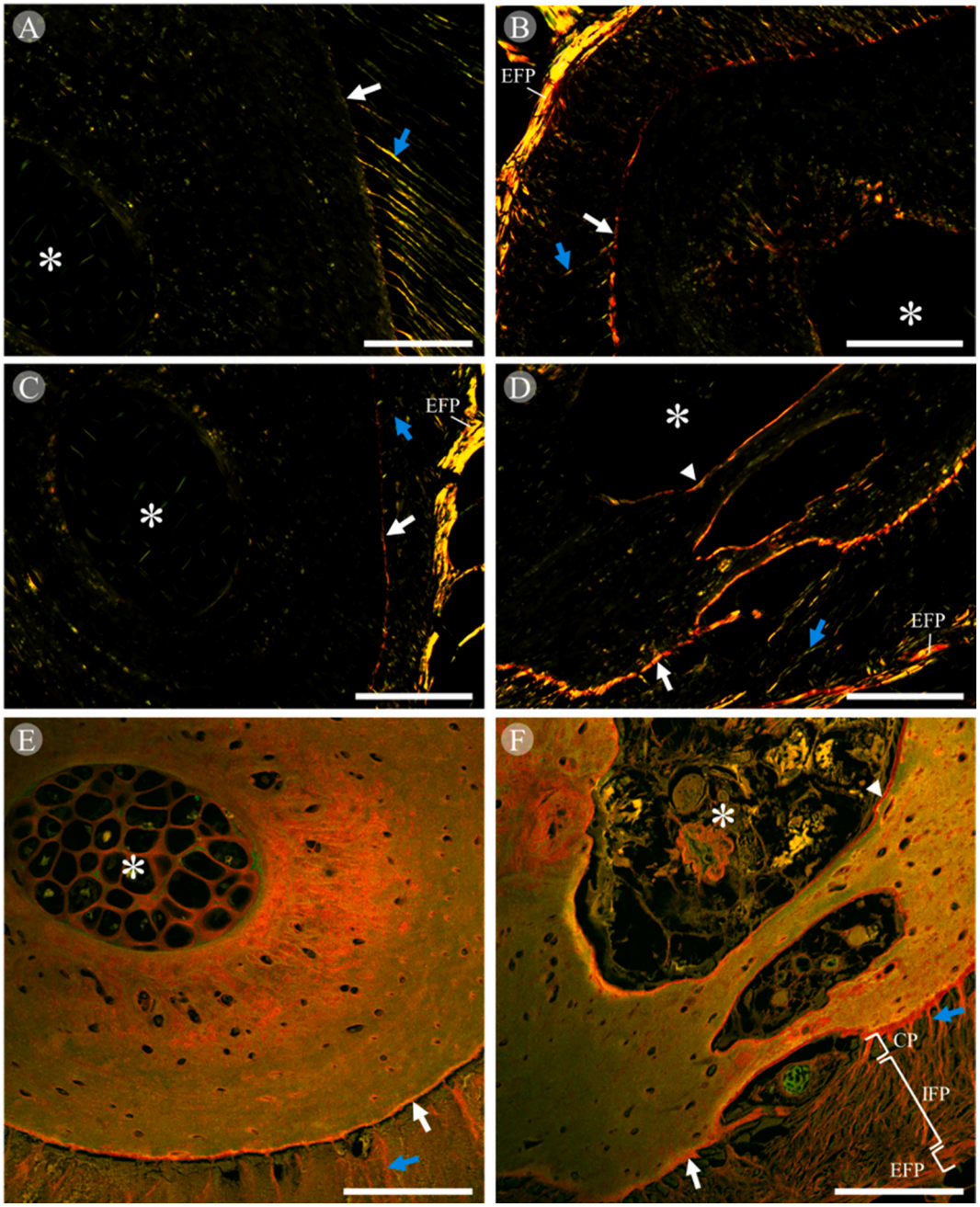

Fig. 3. Collagen distribution in cross-sections of normal (left panel) and abnormal/degenerated (right panel) mid ribs with generalized radiolucency of Atlantic salmon (3 kg). A) to D) under polarized light. E) and F) confocal microscope. Yellow-orange birefringence in polarized images stands for perpendicular collagen type I (thick fibers), while green birefringence perpendicular type III (thin fibers). C) and E), and D) and F) correspond to the same rib, respectively. Picro Sirius red staining. IFP, Interior fibrous periosteum; EFP, Exterior fibrous periosteum. White arrows indicate the external collagen layer of the compact bone under the cellular periosteum (CP). White asterisks indicate either rib core with hyaline-cell (hypertrophic-like) cartilage (normal rib) or a fibrous osteolytic cavity (abnormal/degenerated rib). White arrowheads indicate the internal collagen layer in rib cavities. Blue arrows indicate radial periosteal collagen/Sharpey's fibers. White bars on the bottom right corner of images show the image scale, set to 100 μm. Color print. (For interpretation of the references to color in this figure legend, the reader is referred to the web version of this article.)

perpendicular collagen type I and III fibers (Fig. 2. B and C; Fig. 3. A and C). No blood vessels were observed in the periosteum. Both dietary groups shared no abnormal glycogen accumulation nor significant signs of necrosis and fibrosis in adjacent muscle areas to the ribs. In 8% of the samples, sparse melanomachrophages without near inflammatory processes or fibrosis were seen in deeper layers of the myocommata near blood vessels.

Ribs with abnormal histomorphology exhibited 18–20% greater overall diameter than those with normal histomorphology ($p = 0.04$), and there were no indications of acute or chronic inflammation, melanisation of the ribs or the surrounding soft tissue. The cross-sectional area of the compact bone and osteocyte density were similar for normal and abnormal ribs. However, the hyaline-cell (hypertrophic-like) cartilage rib core possibly degraded/transformed into an irregular cavity of large radiolucency, and an amorphous fibroblasts/fibroblast-like cell network (fibrous rib cavity) with adipose tissue (lipid vacuoles), blood vessels, osteoclasts, and sparse leucocytes (Fig. 4). The rib cavity was surrounded by a thick collagen layer rich in perpendicular

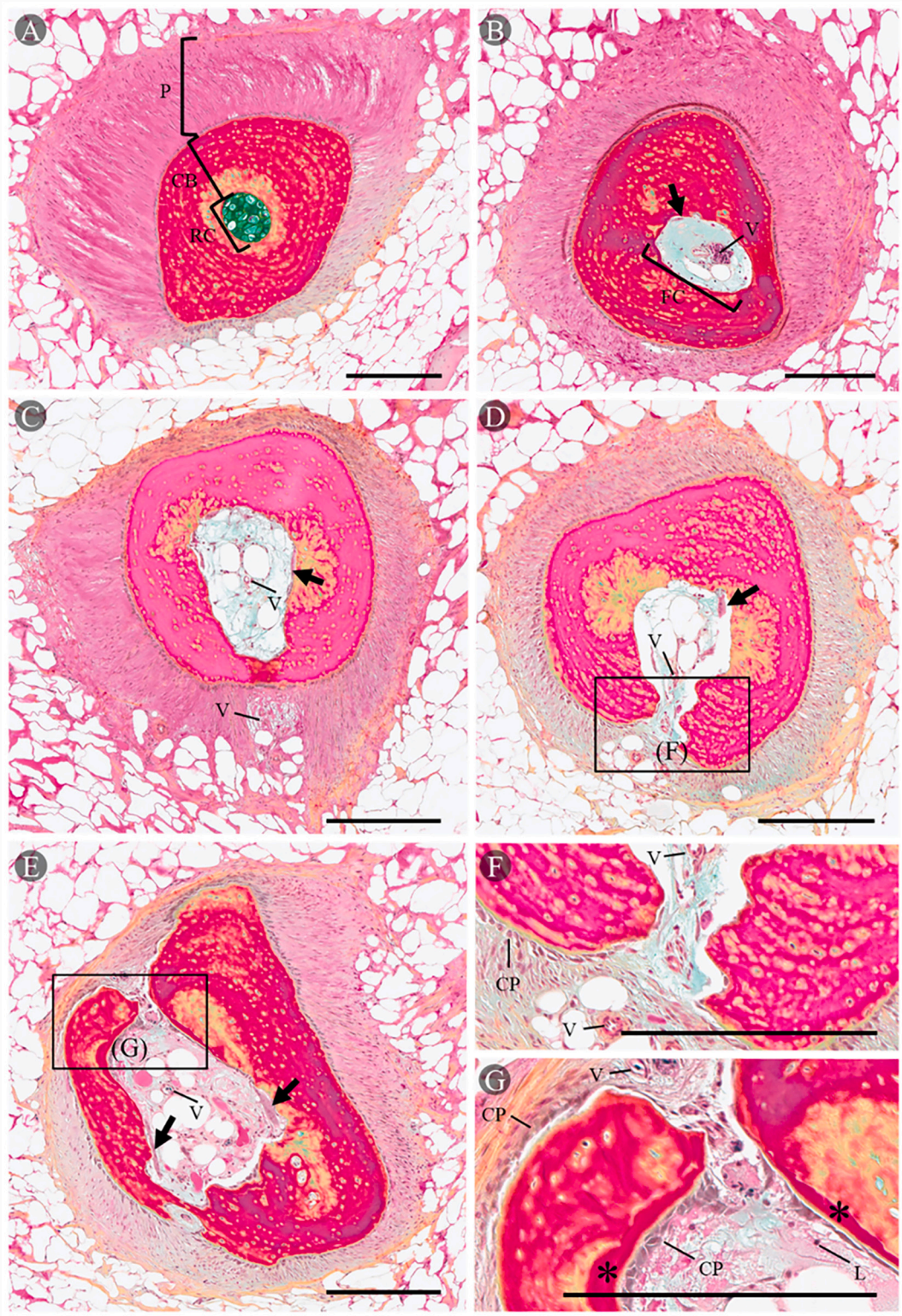

Fig. 4. Proposed model for the cross-sectional progressive degenerative changes of generalized radiolucent ribs of Atlantic salmon (3 kg). A) Grade 0, normal rib; rib core (RC) with hyaline-cell (hypertrophic-like) cartilage. B) Grade 1; first stages of degeneration with increased in rib cross-sectional thickness, abnormal appositional growth, transformation of cartilaginous RC to small fibrous cavity (FC), and mild osteolysis. C) Grade 2; thick rib with large FC, and advanced uneven osteolysis. D) Grade 3; thick rib with large FC and osteolytic opening to the periosteum (P). E) Grade 4; thick rib with large FC, advanced osteolytic opening to P, and infiltration of cellular periosteum (CP). Generalized radiolucency reaches its maximum in grade 4 as it generally depends on the extension and location of the osteolytic areas. Boxes with letters indicate the region of zoom of F) and G). Movat pentachrome staining for proteoglycans and mucins (blue), collagen/reticular fibers (yellow), colocalization of collagen/reticular fibers and proteoglycans (green), muscle and osteoid (or decalcified bone matrix) (reddish-brown), nuclei and elastin (black) and active nucleus (osteoblast in CP) (violet/purple). CB, Compact bone; V, Blood vessels; L, Leucocytes. Black arrows indicate osteoclast. Black asterisks indicate regions with osteomalacia. Black bars on the bottom right corner show the image scale, set to 250 μm. Color print. (For interpretation of the references to color in this figure legend, the reader is referred to the web version of this article.)

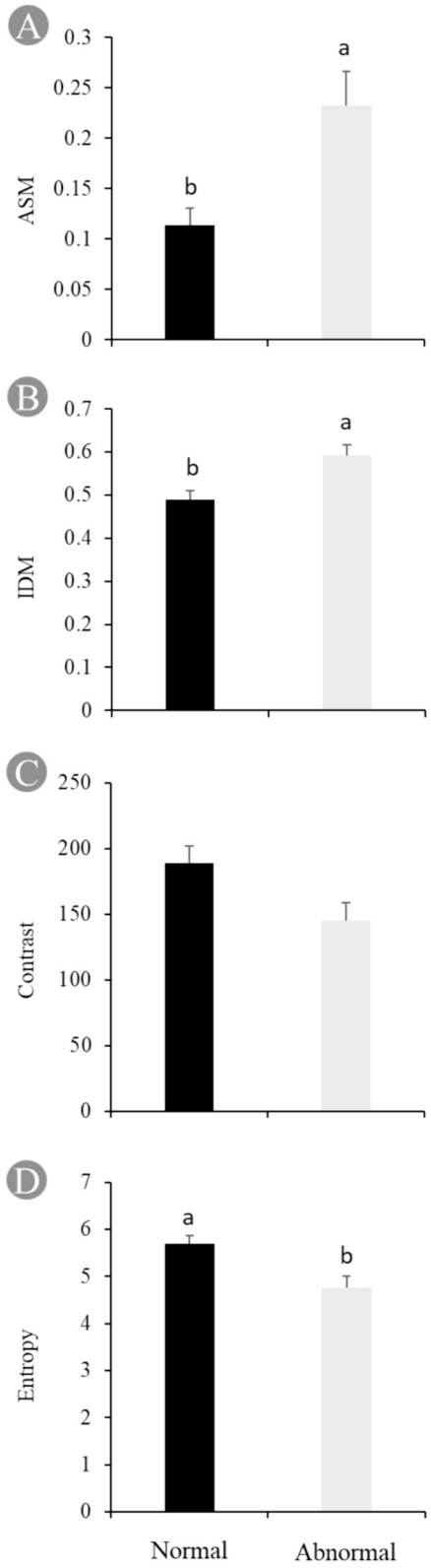

Fig. 5. Quantitative concentric appositional growth pattern of the compact bone from normal and abnormal/degenerative ribs in Atlantic salmon (3 kg). Data is generated through gray level co-occurrence matrix texture analysis of compact bone from histology sections. A) Angular second moment (ASM), B) inverse difference moment (IDM), C) contrast, and D) entropy. Data are presented as non-transformed mean ± SEM, $n = 4$ and 6 for normal and abnormal ribs, respectively. Significant differences between groups are indicated by different letters over the SEM ($p \leq 0.05$).

type I fibers in non-active osteolytic borders (Fig. 3. B and D). Another wide layer of perpendicular type I collagen was observed surrounding the outermost compact bone in contact with the cellular periosteum.

Image texture analyses of rib histology revealed that homogeneity values were found higher in the compact bone of abnormal ribs than normal ribs (ASM, $p = 0.03$; IDM, $p = 0.02$), while heterogeneity values were found lower (Contrast, $p = 0.058$; Entropy, $p = 0.02$) (Fig. 5). Thus, compact bone was more uniform with less gray levels variation in abnormal than normal ribs, hence less organized concentrical osteocyte growth pattern. Notably, the collagen-rich low mineralized halo of slight radiolucency around the chondroid core was reduced in size or appeared with "polar" localization. This was further manifested as isolated islands of disorganized type I and III collagen fibers (none or poor birefringence signal) and glycoprotein composition more visible in the most advanced phases (Fig. 4 and Fig. 6).

Given the common histology features of abnormal ribs, and variable generalized radiolucency affecting 70% of samples accompanied by thickening displayed by X-ray, they were designated as generalized radiolucent ribs. Initial histological changes (Grade 1; Fig. 4. B), included the disappearance of chondrocytes, and the rib core – now cavity – was filled with an amorphous fibrotic substance with lipid vacuoles, accompanied by blood vessels and osteoclasts. The osteolytic changes progressed (Grade 2; Fig. 4. C), and the core penetrated through to the periosteal area (Grade 3; Fig. 4. D and F). Here, the periosteum underwent metaplastic changes, including loss of linear organization of protein fibers and vascularization. The progressive changes were accompanied by loss of linear organization of the concentric appositional growth pattern. Then, cellular periosteum cells infiltrated the osteolytic layer of the cavity, in an endosteum-like manner (Grade 4; Fig. 4. E and G). The different degrees of histomorphology of the compact bone seemed to be positively associated with homogeneity values (Angular second moment, $p = 0.08$; Inverse difference moment, $p = 0.07$), while negatively with heterogeneity (Contrast, $p = 0.02$; Entropy, $p = 0.07$) from the gray level co-occurrence matrix texture analysis. Progressive processes of osteogenesis by appositional growth in the cellular periosteum and osteolysis in the rib cavity likely contributed to the (abnormal) changes in cross-sectional rib morphology, giving a bitubular appearance to ossify the opening by appositional growth (Fig. 6. A). Osteoid was observed in newly formed compact bone (Fig. 4. E and G). Typically, the more advanced the changes, the more visible the generalized radiolucency. Variations to what is described included multiple fibrous rib cavities, and rib core (sometimes exposed to periosteum) containing chondrocytes in the immature hyaline phase (Fig. 6, B, C, and D). As no signs of herniation of the exposed cartilage core were observed in response to internal pressure, it was assumed to be invagination (Fig. 6. C). Although these histological stages were observed in different radiolucent ribs, a combination of some stages could also occur within the same rib (Supplementary 10).

Histologically, red DS were characterized by the presence of intramuscular hemorrhage with infiltration of erythrocytes and inflammatory cells, mainly macrophages. In some cases, melanomachrophages were observed. Black DS presented dispersed melanomacrophages mainly in myocommata and between myocytes in a lower number. Some necrotic myocytes were seen with macrophage infiltration. No major fibrotic areas were observed (Supplementary 11).

3.3. *Dietary effects on fish performance and fillet quality*

The body weight of the V-group was 28% lower compared with the M-group prior to seawater transfer ($p < 0.001$), while the weight difference was 11% in favor of the M-group 10 ten weeks after seawater transfer ($p = 0.003$). At harvesting, the weight of both dietary groups was similar (Table 2), but the condition factor of the V-group was slightly higher ($p = 0.02$). The mortality rate of both dietary groups was similar (< 1%). Fillet quality analyses at harvest revealed comparable color intensity of both dietary groups (Score; 23.5–23.7), but the V-

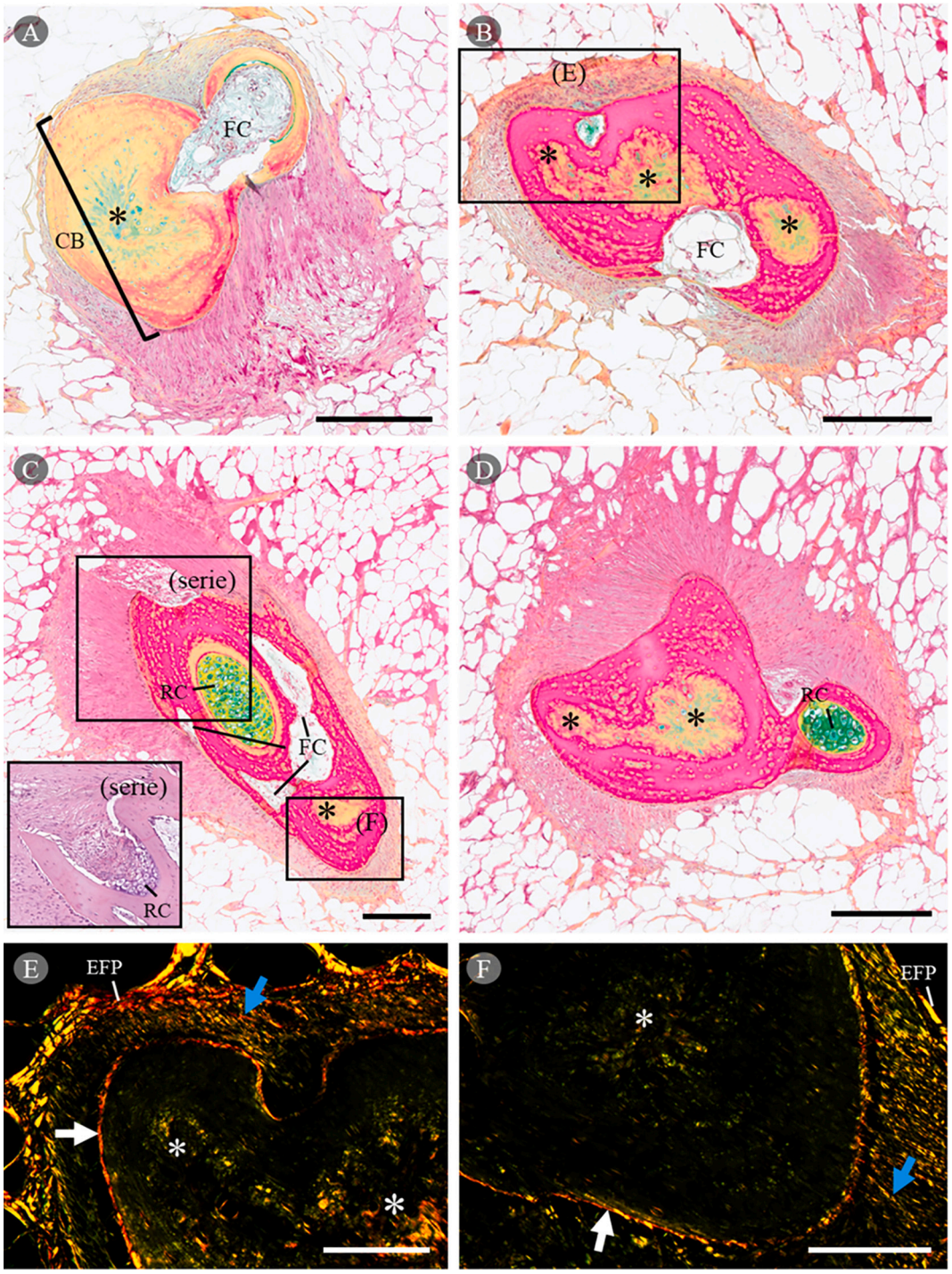

Fig. 6. Alternative cross-sectional morphologies for advanced degenerative stages of generalized radiolucent ribs with cores (RC) of cell-rich (immature-like) hyaline cartilage and fibrous cavity (FC) in Atlantic salmon (3 kg). A) to D) Movat pentachrome staining for proteoglycans and mucins (blue), collagen/reticular fibers (yellow), colocalization of collagen/reticular fibers and proteoglycans (green), muscle and osteoid (or decalcified bone matrix) (reddish-brown), nuclei and elastin (black) and active nucleus (osteoblast in cellular periosteum) (violet/purple). Boxes with letters on images B) and C) indicate the region of zoom of images E) and F). Serie histology image in Haematoxylin and Eosin. Black bars on the bottom right corner from A) to D) show the image scale, set to 250 μm. E) and F) Picro Sirius red staining under polarized light. Yellow-orange birefringence in polarized images stands for perpendicular collagen type I (thick fibers), while green birefringence perpendicular type III (thin fibers). EFP, Exterior fibrous periosteum. White arrows indicate the external collagen layer of the compact bone (CB). Blue arrows indicate radial periosteal collagen/Sharpey's fibers. Black and white asterisks indicate regions of the CB rich in collagen and glycoproteins. White bars on the bottom right corner of E) and F) images show the image scale, set to 100 μm. Color print. (For interpretation of the references to color in this figure legend, the reader is referred to the web version of this article.)

group had a higher gaping score ($p = 0.03$) and softer fillets ($p = 0.049$) than the M-group (Table 2).

3.4. Bone mechanical properties

Mechanical tests of salmon ribs revealed a decreasing breaking load from proximal to distal rib parts, with no differences between dietary groups (Table 1). The elasticity showed a similar trend with lower values at the proximal than mid and distal rib parts. Mechanical rib analyses showed no significant differences between the dietary groups, but the V-group showed a numerically higher elasticity ($p = 0.06$) than the M-group in mid rib parts (Table 1).

The area and load of vertebrae were lower of the V-group than the M-group at 5, 10, 15, and 20% compression depth ($p < 0.04$). These values increased with compression depth for both groups (Supplementary 12). Among all compression depths, only elasticity at 15% was different between dietary groups, with higher modulus in the V-group than M-group (136.8 ± 5.1 vs. 121.9 ± 5 N/mm; $p = 0.045$).

Assuming no body weight and diet interaction, the most significant correlations with rib morphology were between the number of ribs with axis deviations per rib cage side and either area ($r = -0.37$; $p = 0.049$), load ($r = -0.38$; $p = 0.04$) at 5%, or area ($r = -0.37$; $p = 0.04$) at 10% of compression depth of vertebrae. Regarding rib mechanical properties, the most significant correlations were between the modulus of elasticity in mid rib parts and either area ($r = 0.36$; $p = 0.02$) or load ($r = 0.32$; $p = 0.03$) at 15% of the compression depth of vertebrae.

3.5. Bone mineral content

No differences were observed in the composition of macrominerals in ribs between the dietary groups, although the V-group tended to have a lower P concentration than the M-group ($p = 0.07$) (Table 1).

There were only few significant differences in the mineral composition of vertebrae between the dietary groups. Fish prior to seawater transfer showed a higher % of ash with a higher Ca:P ratio ($p = 0.03$), Na ($p = 0.01$), and Mn levels ($p = 0.02$) in the V-group than in the M-group (Supplementary 3). At harvest, the mineral analysis revealed a higher Na content in the V-group than in the M-group ($p = 0.002$) (Supplementary 12).

3.6. Blood serum

Prior to seawater transfer, the serum from the M-group showed higher levels of ALP ($p = 0.01$), creatinine ($p < 0.001$), cholesterol ($p < 0.001$), and free fatty acids ($p = 0.02$) than the V-group (Supplementary 13). Ten weeks after seawater transfer, only ALP levels differed significantly between the fish group, being higher for the V-group than the M-group ($p < 0.001$). At harvest, all blood parameters were similar for the dietary groups (Supplementary 13).

3.7. Focal dark spots

At harvest, fish presented DS. No differences were observed in the prevalence of red (5%) or black DS (3–12%) between the dietary groups. DS were primarily found in the form of petechial, focal hemorrhages, and mild melanisation (score 0.5–1), which is generally not considered a cause for quality downgrading (Supplementary 14).

4. Discussion

In the present study, we could confirm and describe the dominance of two subtypes of rib abnormalities in Atlantic salmon which additionally are particularly sensitive to the composition of the diet during smoltification. On the one hand, axis deviations such as parallel deformation of several mid rib parts resulting from mechanical deformations of the rib cage (Jiménez-Guerrero et al., 2022) and wrinkly ribs, earlier associated with suboptimal (P-deficient) diet (Baeverfjord et al., 1998). On the other hand, generalized radiolucent ribs previously related to seawater transfer and osteolytic secondary changes due to a local inflammatory process such as DS (Jiménez-Guerrero et al., 2022). Generalized radiolucent ribs showed consistent histological characteristics across our samples with no surrounding local inflammatory process or DS. Here, the hyaline-cell cartilage rib core degraded, evolving into an expanded osteolytic and fibrotic cavity with internal lipid vacuoles (Witten et al., 2010), and vascularization that possibly led to the increase in rib diameter through compensatory appositional growth to preserve the mechanical properties. In the most likely scenario, the presence of non-cartilage tissue in the rib cavity represents the transformation of chondrocytes to mesenchymal-like cells (de la Fuente et al., 2004; Giovannone et al., 2019; Witten et al., 2010) (e.g., fibroblast, adipocytes, and endothelial cells). Blood supply to the rib and internal vascularization is likely an essential step for rib core degradation and the progression of generalized radiolucency, by facilitating the first core infiltration of myeloid-like cells (e.g., osteoclasts and lymphocytes) (Veis and O'Brien, 2023). On the one hand, as observed by Brimsholm et al. (2023), blood vessels in periosteum and rib cavities may naturally exist and, though not showed, have access to the rib core by rib head or openings along the compact bone. They suggested that rib core degradation and vascularization could be mere anatomical variations in salmon ribs because of the aquatic environment, similar to other marine species where bone degradation may be expected in late growth phases (Soliman, 2018). On the other hand, our systematic study showed vascularized periosteum and core exclusively in radiolucent ribs, suggesting that along the rib length, generalized radiolucency might have induced metaplastic changes in the periosteum followed by neovascularization. Hence, the initial osteolysis along the rib could have either been initiated from anatomical vessel connections or emerged from a vascularization event in a specific rib region. In the later scenario, the compact bone would experience an initial osteolysis from the periosteum side.

Our findings indicate clear evidence of pathology in generalized radiolucency, particularly in advanced stages where morphological alterations align with discernible X-ray changes. Jiménez-Guerrero et al. (2022) found that generalized radiolucency prevalence is notably low in adult wild fish, and it does not increase in later growth stages in farmed fish, indicating that these changes are not associated with late growth phases. On the contrary, there is a response to environmental factors and dietary differences. Combined with the histopathological changes, altered rib development, degeneration, and possibly osteomalacia seemed to be the likely diagnosis of generalized radiolucent ribs when there was no associated local inflammatory process. Osteomalacia was also supported by the increase of periosteal collagen, possibly in an attempt to compensate for the observed higher elasticity and the lower P content in ribs. Softer ribs might also be contributed by the relative increase of the fibrotic cavity, osteoid, and distortion of the concentric mineralized layers or disorganized collagen-rich islands in the compact bone, which would increase the risk of rib deformations (axis deviations), and, therefore, clinical relevance as our data shows. When selecting ribs for assessing elasticity and P deficiencies, we could not discriminate between normal and abnormal ribs by visual inspection, which resulted in an increased standard deviation that impacted significance levels between dietary groups. Because distal rib parts that concentrate most rib abnormalities have the weakest breaking load and relatively higher elasticity than proximal parts, it reinforces that mid and predominantly distal areas of the rib cage are more susceptible to external mechanical stress (Jiménez-Guerrero et al., 2022).

To understand the observed long-term effects of dietary differences on rib morphology in the broader musculoskeletal framework, we additionally explored the growth performance, vertebral health, and skeletal muscle. The initial poor growth of the V-group was likely a response to the lower muscle development. The poor performance was unlikely due exclusively to a P deficiency (Baeverfjord et al., 1998; Drábiková et al., 2021), but possibly as a response to the suboptimal

level of methionine in the V-group diet (0.7 vs. 0.9–1.1 g/100 g) (Hua and Bureau, 2019; Mai et al., 2022) among other nutritional differences such as EPA and DHA, which were under recommended levels for maximizing growth performance (< 0.1–0.2 vs. 0.5 g/100 g of lipids) (Qian et al., 2020). At the end of the experiment, despite significant deterioration in rib health observed in the V-group, it displayed compensatory growth. This enabled both groups to demonstrate similar traits at harvest, including body weight, fillet color, and serum chemistry. These findings evidence the remarkable compensatory abilities of salmon. Therefore, the effects of dietary differences in growth would not have been detected in our fish by standard evaluations at the slaughterhouse.

As vertebrae morphology and composition are proved markers of skeleton health in salmon, they were monitored in the period prior to and after seawater transfer, and at harvest. As expected in the short-term (Drábiková et al., 2021, 2022; Fjelldal et al., 2012), we found a similarly low number of morphological vertebral abnormalities prior to and after seawater in both salmon groups. Additionally serum P*i* concentrations of both groups were similar to fish fed a regular P diet in Drábiková et al. (2021), suggesting that dietary P*i* might have been absorbed and made available at similar levels. This was also supported by the lack of observable effects on the width of the intervertebral space between the M- and V-groups, a short-term indicator of P deficiency as noted by Drábiková et al. (2021). Despite these similarities, we identified differences in bone mineralization in response to dietary differences, as indicated by the lower vertebra X:Y ratio in the V-group before and after seawater transfer. Before the transfer, lower vertebra X:Y differences did not correspond to variations in mineral composition (excluding Ca:P ratio, Na, and Mn) or clinically observable impaired bone mineralization. Intriguingly, the gutted body of the V-group had a higher ash content even though the fish were fed lower ash levels than the M-group during smoltification. As these mineral composition results are not specific to the bone, it is important to consider other factors, such as a relatively lower mineral concentration in fast-growing fish (Baeverfjord et al., 2018).

Ten weeks after seawater transfer, vertebra X:Y ratio and macroscopic evaluations indicated that both groups went through a period in which they were in negative bone mineralization balance. The effects of seawater transfer in vertebrae of both farmed and wild salmon have already been reported (Fjelldal et al., 2006; Fjelldal et al., 2007). Later, Jiménez-Guerrero et al. (2022) also reported signs of negative mineralization balance in ribs after seawater transfer. Here, we show that the observed short-term impaired mineralization generally impacted the V-group more as they likely started with a subclinical lower mineral status prior to seawater transfer. However, the impaired vertebral mineralization was resolved, and both groups presented similar normal vertebral morphology and mineral composition at harvest (excluding Na) (Drábiková et al., 2021, 2022), contrasting to what Fjelldal et al. (2009) reported. Therefore, contrary to what was found in ribs, the impaired mineralization did not cross the point of no return, as the number of fish with vertebral abnormalities did not differ between the dietary groups in the long-term. Such bone development behavior was in line with serum ALP (osteoblast activity), which showed lower values in the V-group than the M-group prior to seawater transfer, followed by an inversion of the trend 10 weeks after seawater transfer. The ALP pattern is probably a sign of compensatory skeleton growth with a recovery to similar values at harvest. Nevertheless, besides the lack of clinical evidence, there were subclinical long-term effects on the mechanical properties of the trabecular fraction of vertebrae.

The higher concentration of Na in the vertebrae composition of the V-group at harvest was in accordance with our findings in body composition prior to seawater transfer, and it establishes a link between high levels of Na in bone composition and long-term deterioration of the mechanical properties, morphology, and composition of ribs and mechanical properties of vertebral trabeculae. Potential stimulatory effects of Na-based hydroxyapatite on bone osteolysis and remodeling due to its higher instability likely affected the mechanical properties of compact bone (Yoo et al., 2021). Unfortunately, we did not have enough material to determine Na concentrations in rib bones, which would strengthen these findings. Factors modulating Na concentrations in fish bones and their impact on skeleton health should be the focus of future research.

Regarding the skeletal muscle, we present the first evidence for long-term effects (beyond three weeks; Kaushik et al. (1995)) of dietary differences during smoltification on muscle quality in salmon at harvest. Thus, we hypothesize a response of the diet near seawater transfer on DS at harvest, as Sissener et al. (2016) reported, although red and black DS of lower prevalence and economic relevance than previously reported in commercial sea-cages were found (Bjørgen et al., 2019; Jiménez-Guerrero et al., 2022). Moreover, the lack of effects in DS did not correspond to the modified number of ribs with axis deviations and mechanical properties of ribs. Here, these rib axis deviations were mostly contributed by wrinkly malformations resulting from impaired mineralization rather than traumatic events, which may explain the lack of relationship. On the other hand, it is possible that a low incidence of damaging mechanical impacts on the rib cage in our small-scale experimental conditions made it difficult to evaluate any difference between the dietary groups. Altogether, we cannot exclude the potential protective effects of nutrition during smoltification on musculoskeletal health against DS in more challenging environments.

Although the dietary treatments did not aim to be comparable to commercial diets, we found the marine-based diet to have positive effects on rib development. Compared to a previous study (Jiménez-Guerrero et al., 2022), we observed a similar number for most rib abnormalities in the M-group as in wild fish. We could also see a reduction of the characteristic concentration of rib abnormalities in central parts of the rib cage in the M-group, drawing a similar pattern as for wild fish. Moreover, the M-group showed a 33% and 50% lower number of axis deviations compared with salmon fed a standard diet and grown in land-based tanks or sea-cages respectively.

Several factors may explain the positive effects of high dietary inclusion of marine ingredients during smoltification. For example nutritional deficiencies could explain the observed increase in axis deviations in ribs due to structural defects during early development. However, the degeneration and possibly long-term osteomalacia in ribs after fish were fed commercial diets suggests persistent changes in either osteogenesis or absorption of nutrients after the dietary treatment. The parallel affection of the mechanical properties of skeletal muscle and bone suggests a generalized alteration of the extracellular collagen matrix, which is known to be mediated by collagen type I (Aubin, 1998) and collagen type II alpha 1 chain *(col2a1)* (Dale and Topczewski, 2011) among other genes. In teleost, there are three type I collagens, alpha 1a (*col1a1a*), 1b (*col1a1b*) and 2 (*col1a2*) chains (Gistelinck et al., 2016; Morvan-Dubois et al., 2003). Although little literature is available, while *col1a1* can be upregulated by n − 3 PUFAs (Abshirini et al., 2021; Ytteborg et al., 2015), *col2a1* is downregulated when using vegetal-based protein concentrates in diet (Dhanasiri et al., 2020). Transformation or dedifferentiation, feasible in mesenchymal lineage cells, could be induced through dietary-dependent or mechanical factors (Hall, 2015); in fact, n − 3 PUFAs have been proven to suppress collagen matrix degradation in cartilage (Abshirini et al., 2021), which would explain the lower fibrotic changes in cartilage rib cores in the M-group. Thus, combining fish oil and non-vegetal-based protein concentrates probably had a synergic effect on musculoskeletal health. We recommend further investigation into the potential nutritional programming effects of incorporating a high proportion of marine-based ingredients in the diets of farmed salmon, particularly during the smoltification phase.

5. Conclusions

Generalized radiolucency and axis deviation are the two major types of morphological abnormalities in salmon ribs. Salmon rib morphology was more sensitive to the smoltification diet than vertebrae. Generalized

radiolucent ribs were characterized by different forms of altered rib development, degeneration, and possibly osteomalacia.

Declaration of funding

The study was supported by the Norwegian Seafood Research Fund (FHF) (901487), and the Norwegian University of Life Sciences (NMBU).

CRediT authorship contribution statement

Raúl Jiménez-Guerrero: Writing – review & editing, Writing – original draft, Visualization, Validation, Methodology, Investigation, Formal analysis, Data curation. **Grete Baeverfjord:** Writing – review & editing, Visualization, Validation, Supervision, Resources, Project administration, Methodology, Investigation, Conceptualization. **Øystein Evensen:** Writing – review & editing, Supervision, Methodology, Investigation. **Turid Mørkøre:** Writing – review & editing, Visualization, Validation, Supervision, Resources, Project administration, Methodology, Investigation, Formal analysis, Conceptualization.

Declaration of competing interest

Turid Mørkøre reports financial support was provided by Norwegian Seafood Research Fund.

Data availability

Data will be made available on request.

Acknowledgments

The Norwegian Seafood Research Fund (FHF) and Norwegian University of Life Sciences (NMBU) supported this study. The authors acknowledge the skillful assistance, dedicated fish management, and excellent work provided by staff at the Research Station for Sustainable Aquaculture (Nofima) and laboratories, with special thanks to Kjellrun Hoås Gannestad. Thanks to Ph. D. Thomas Larsson and M.Sc. Sumeng Galdat, for your assistance in processing part of the data. Thanks to Miroslava Hansen for the excellent work processing and sectioning histology samples. Thanks to The Imaging Center (NMBU) for allowing the use of its infrastructure and expertise.

Appendix A. Supplementary data

Supplementary data to this article can be found online at https://doi.org/10.1016/j.aquaculture.2024.741140.

References

Abshirini, M., Ilesanmi-Oyelere, B.L., Kruger, M.C., 2021. Potential modulatory mechanisms of action by long-chain polyunsaturated fatty acids on bone cell and chondrocyte metabolism. Prog. Lipid Res. 83, 101113 https://doi.org/10.1016/j.plipres.2021.101113.

Akama, K., Ebata, K., Maeno, A., Taminato, T., Otosaka, S., Gengyo-Ando, K., Nakai, J., Yamasu, K., Kawamura, A., 2020. Role of somite patterning in the formation of Weberian apparatus and pleural rib in zebrafish. J. Anat. 236 (4), 622–629. https://doi.org/10.1111/joa.13135.

Andersen, B.U., Steinsholt, K., Stroemsnes, A.N., Thomassen, M.S., 1994. Fillet gaping in farmed Atlantic salmon (*Salmo Salar*). Nor. J. Agric. Sci. 8 (3/4), 165–179. https://nmbu.brage.unit.no/nmbu-xmlui/handle/11250/3006394.

AOCSBa6a-05, 2017. Official methods and recommended practices of the AOCS - Determination of crude fiber. https://myaccount.aocs.org/PersonifyEbusiness/Store/Product-Details/productId/111455.

Aubin, J.E., 1998. Bone stem cells. J. Cell. Biochem. Suppl. 30-31, 73–82. https://pubmed.ncbi.nlm.nih.gov/9893258/.

Baeverfjord, G., Asgard, T., Shearer, K.D., 1998. Development and detection of phosphorus deficiency in Atlantic salmon, *Salmo salar* L., parr and post-smolts. Aquacult. Nutr. 4 (1), 1–11. https://doi.org/10.1046/j.1365-2095.1998.00095.x.

Baeverfjord, G., Antony Jesu Prabhu, P., Fjelldal, P.G., Albrektsen, S., Hatlen, B., Denstadli, V., Ytteborg, E., Takle, H., Lock, E.-J., Berntssen, M.H.G., Lundebye, A.-K., Åsgård, T., Waagbø, R., 2018. Mineral nutrition and bone health in salmonids. Rev. Aquac. 11 (3), 740–765. https://doi.org/10.1111/raq.12255.

Baird, M.F., Graham, S.M., Baker, J.S., Bickerstaff, G.F., 2012. Creatine-kinase- and exercise-related muscle damage implications for muscle performance and recovery. J. Nutr. Metab. 2012, 960363 https://doi.org/10.1155/2012/960363.

Bjørgen, H., Haldorsen, R., Oaland, Ø., Kvellestad, A., Kannimuthu, D., Rimstad, E., Koppang, E.O., 2019. Melanized focal changes in skeletal muscle in farmed Atlantic salmon after natural infection with *piscine orthoreovirus* (PRV). J. Fish Dis. 42 (6), 935–945. https://doi.org/10.1111/jfd.12995.

Bou, M., Berge, G.M., Baeverfjord, G., Sigholt, T., Østbye, T.K., Ruyter, B., 2017. Low levels of very-long-chain n-3 PUFA in Atlantic salmon (*Salmo salar*) diet reduce fish robustness under challenging conditions in sea cages. J. Nutr. Sci. 6, e32 https://doi.org/10.1017/jns.2017.28.

Brimsholm, M., Fjelldal, P.G., Hansen, T., Trangerud, C., Knutsen, G.M., Asserson, C.F., Koppang, E.O., Bjørgen, H., 2023. Anatomical and pathological characteristics of ribs in the Atlantic salmon (*Salmo salar* L.) and its relevance to soft tissue changes. Anat. Histol. Embryol. https://doi.org/10.1111/ahe.12900.

Clarke, W.C., Saunders, R.L., McCormick, S.D., 1996. Smolt production. In: Pennel, W., Barton, B.A. (Eds.), Principles of Salmonid Culture. CRC Press, Elsevier, Amsterdam, The Netherlands, pp. 517–567. https://shop.elsevier.com/books/principles-of-salmonid-culture/pennell/978-0-444-82152-2.

Cohen, L., Dean, M., Shipov, A., Atkins, A., Monsonego-Ornan, E., Shahar, R., 2012. Comparison of structural, architectural and mechanical aspects of cellular and acellular bone in two teleost fish. J. Exp. Biol. 215 (11), 1983–1993. https://doi.org/10.1242/jeb.064790.

Currey, J.D., 2003. The many adaptations of bone. J. Biomech. 36 (10), 1487–1495. https://doi.org/10.1016/s0021-9290(03)00124-6.

Dale, R.M., Topczewski, J., 2011. Identification of an evolutionarily conserved regulatory element of the zebrafish *col2a1a* gene. Dev. Biol. 357 (2), 518–531. https://doi.org/10.1016/j.ydbio.2011.06.020.

De Clercq, A., Perrott, M.R., Davie, P.S., Preece, M.A., Wybourne, B., Ruff, N., Huysseune, A., Witten, P.E., 2017. Vertebral column regionalisation in Chinook salmon, *Oncorhynchus tshawytscha*. J. Anat. 231 (4), 500–514. https://doi.org/10.1111/joa.12655.

de la Fuente, R., Abad, J.L., García-Castro, J., Fernández-Miguel, G., Petriz, J., Rubio, D., Vicario-Abejón, C., Guillén, P., González, M.A., Bernad, A., 2004. Dedifferentiated adult articular chondrocytes: a population of human multipotent primitive cells. Exp. Cell Res. 297 (2), 313–328. https://doi.org/10.1016/j.yexcr.2004.02.026.

Dhanasiri, A.K.S., Johny, A., Xue, X., Berge, G.M., Bogevik, A.S., Rise, M.L., Fæste, C.K., Fernandes, J.M.O., 2020. Plant-based diets induce transcriptomic changes in muscle of zebrafish and Atlantic Salmon. Front. Genet. 11 https://doi.org/10.3389/fgene.2020.575237.

Drábiková, L., Fjelldal, P.G., De Clercq, A., Yousaf, M.N., Morken, T., McGurk, C., Witten, P.E., 2021. Vertebral column adaptations in juvenile Atlantic salmon *Salmo salar*, L. as a response to dietary phosphorus. Aquac. 541, 736–776. https://doi.org/10.1016/j.aquaculture.2021.736776.

Drábiková, L., Fjelldal, P.G., De Clercq, A., Yousaf, M.N., Morken, T., McGurk, C., Witten, P.E., 2022. What will happen to my smolt at harvest? Individually tagged Atlantic salmon help to understand possible progression and regression of vertebral deformities. Aquac. 559, 738430 https://doi.org/10.1016/j.aquaculture.2022.738430.

EC152, 2009. Commission Regulation (EC) No 152/2009 of 27 January 2009 laying down the methods of sampling and analysis for the official control of feed (Text with EEA relevance), 130. https://eur-lex.europa.eu/legal-content/EN/ALL/?uri=CELEX%3A32009R0152.

Fjelldal, P.G., Lock, E.-J., Grotmol, S., Totland, G.K., Nordgarden, U., Flik, G., Hansen, T., 2006. Impact of smolt production strategy on vertebral growth and mineralisation during smoltification and the early seawater phase in Atlantic salmon (*Salmo salar*, L.). Aquac. 261 (2), 715–728. https://doi.org/10.1016/j.aquaculture.2006.08.008.

Fjelldal, P.G., Nordgarden, U., Hansen, T., 2007. The mineral content affects vertebral morphology in underyearling smolt of Atlantic salmon (*Salmo salar* L.). Aquac. 270 (1), 231–239. https://doi.org/10.1016/j.aquaculture.2007.03.008.

Fjelldal, P.G., Hansen, T., Breck, O., Sandvik, R., Waagbø, R., Berg, A., Ørnsrud, R., 2009. Supplementation of dietary minerals during the early seawater phase increase vertebral strength and reduce the prevalence of vertebral deformities in fast-growing under-yearling Atlantic salmon (*Salmo salar* L.) smolt. Aquacult. Nutr. 15 (4), 366–378. https://doi.org/10.1111/j.1365-2095.2008.00601.x.

Fjelldal, P.G., Hansen, T., Albrektsen, S., 2012. Inadequate phosphorus nutrition in juvenile Atlantic salmon has a negative effect on long-term bone health. Aquac. 334-337, 117–123. https://doi.org/10.1016/j.aquaculture.2011.12.043.

Gil Martens, L., Witten, P.E., Fivelstad, S., Huysseune, A., Sævareid, B., Vikeså, V., Obach, A., 2006. Impact of high water carbon dioxide levels on Atlantic salmon smolts (*Salmo salar* L.): effects on fish performance, vertebrae composition and structure. Aquac. 261 (1), 80–88. https://doi.org/10.1016/j.aquaculture.2006.06.031.

Giovannone, D., Paul, S., Schindler, S., Arata, C., Farmer, D.T., Patel, P., Smeeton, J., Crump, J.G., 2019. Programmed conversion of hypertrophic chondrocytes into osteoblasts and marrow adipocytes within zebrafish bones. Elife 8. https://doi.org/10.7554/eLife.42736.

Gislason, H., Karstensen, H., Christiansen, D., Hjelde, K., Helland, S., Bæverfjord, G., 2010. Rib and vertebral deformities in rainbow trout (*Oncorhynchus mykiss*) explained by a dominant-mutation mechanism. Aquac. 309 (1), 86–95. https://doi.org/10.1016/j.aquaculture.2010.09.016.

Gistelinck, C., Gioia, R., Gagliardi, A., Tonelli, F., Marchese, L., Bianchi, L., Landi, C., Bini, L., Huysseune, A., Witten, P.E., Staes, A., Gevaert, K., De Rocker, N., Menten, B., Malfait, F., Leikin, S., Carra, S., Tenni, R., Rossi, A., De Paepe, A.,

Coucke, P., Willaert, A., Forlino, A., 2016. Zebrafish collagen type I: molecular and biochemical characterization of the major structural protein in bone and skin. Sci. Rep. 6 (1), 21540. https://doi.org/10.1038/srep21540.
Gray, J., 1957. How fishes swim. Sci. Am. 197 (2), 48–55. http://www.jstor.org/stable/24940913.
Hall, B.K., 2015. Chapter 30 - initiating skeletal growth. In: Hall, B.K. (Ed.), Bones and Cartilage. Academic Press, San Diego, pp. 475–486. https://doi.org/10.1016/B978-0-12-416678-3.00030-6.
Hansen, T., Fjelldal, P.G., Yurtseva, A., Berg, A., 2010. A possible relation between growth and number of deformed vertebrae in Atlantic salmon (*Salmo salar* L.). J. Appl. Ichthyol. 26 (2), 355–359. https://doi.org/10.1111/j.1439-0426.2010.01434.x.
Haugarvoll, E., Bjerkas, I., Szabo, N.J., Satoh, M., Koppang, E.O., 2010. Manifestations of systemic autoimmunity in vaccinated salmon. Vaccine 28 (31), 4961–4969. https://doi.org/10.1016/j.vaccine.2010.05.032.
Horton, J.M., Summers, A.P., 2009. The material properties of acellular bone in a teleost fish. J. Exp. Biol. 212 (9), 1413–1420. https://doi.org/10.1242/jeb.020636.
Hua, K., Bureau, D.P., 2019. Estimating changes in essential amino acid requirements of rainbow trout and Atlantic salmon as a function of body weight or diet composition using a novel factorial requirement model. Aquac. 513, 734440 https://doi.org/10.1016/j.aquaculture.2019.734440.
ISO13903, 2005. Animal feeding stuffs - Determination of amino acids content, p. 17. https://www.iso.org/standard/37258.html.
ISO5983-2, 2009. Animal feeding stuffs - Determination of nitrogen content and calculation of crude protein content - Part 2: Block digestion and steam distillation method, 15. https://www.iso.org/standard/39160.html.
ISO5984, 2002. Animal feeding stuffs - Specifies a method for the determination of crude ash of animal feeding stuffs, p. 6. https://www.iso.org/standard/37272.html.
ISO6491, 1998. Animal feeding stuffs - Determination of phosphorus content - Spectrometric method, p. 7. https://www.iso.org/standard/12864.html.
ISO6496, 1999. Animal feeding stuffs - Preparation of test samples - Determination of moisture and other volatile matter content, p. 7. https://www.iso.org/obp/ui/en/#iso:std:iso:6496:ed-2:v1:en.
ISO6878, 2004. Water quality - Determination of phosphorus - Ammonium molybdate spectrometric method, p. 21. https://www.iso.org/standard/36917.html.
ISO9831, 1998. Animal feeding stuffs - Determination of gross calorific value - Bomb calorimeter method, p. 23. https://www.iso.org/standard/17702.html.
Jiao, Y.Y., Okada, M., Hara, E.S., Xie, S.C., Nagaoka, N., Nakano, T., Matsumoto, T., 2020. Micro-architectural investigation of teleost fish rib inducing pliant mechanical property. Materials 13 (22), 5099. https://doi.org/10.3390/ma13225099.
Jiménez-Guerrero, R., Baeverfjord, G., Evensen, Ø., Hamre, K., Larsson, T., Dessen, J.-E., Gannestad, K.-H., Mørkøre, T., 2022. Rib abnormalities and their association with focal dark spots in Atlantic salmon fillets. Aquac. 561, 738697 https://doi.org/10.1016/j.aquaculture.2022.738697.
Karki, R., 2022. Effect of Dietary Protein and Lipid Sources on Technical Quality of Pellets for Atlantic Salmon. Norwegian University of Life Sciences, Ås. https://nmbu.brage.unit.no/nmbu-xmlui/handle/11250/2999851.
Kaushik, S.J., Cravedi, J.P., Lalles, J.P., Sumpter, J., Fauconneau, B., Laroche, M., 1995. Partial or total replacement of fish meal by soybean protein on growth, protein utilization, potential estrogenic or antigenic effects, cholesterolemia and flesh quality in rainbow trout, *Oncorhynchus mykiss*. Aquac. 133 (3), 257–274. https://doi.org/10.1016/0044-8486(94)00403-B.
Kryvi, H., Poppe, L.T., 2016. Fiskeanatomi. Fagbokforlaget, Bergen. https://www.fagbokforlaget.no/Fiskeanatomi/I9788245037333.
Kuo, T.-R., Chen, C.-H., 2017. Bone biomarker for the clinical assessment of osteoporosis: recent developments and future perspectives. Biomark. Res. 5 (1), 18. https://doi.org/10.1186/s40364-017-0097-4.
Mai, K., Xue, M., He, G., Xie, S.Q., Kaushik, S.J., 2022. Chapter 4 - protein and amino acids. In: Hardy, R.W., Kaushik, S.J. (Eds.), Fish Nutrition, Fourth edition. Academic Press, pp. 181–302. https://doi.org/10.1016/B978-0-12-819587-1.00012-4.
Mørkøre, T., 2012. Filet av oppdrettslaks: Kvalitetsavvik og årsakssammenhenger. Nofima 12, 1–59. https://nofima.no/publikasjon/1154001/.
Mørkøre, T., Einen, O., 2003. Relating sensory and instrumental texture analyses of Atlantic salmon. J. Food Sci. 68 (4), 1492–1497. https://doi.org/10.1111/j.1365-2621.2003.tb09672.x.
Morvan-Dubois, G., Le Guellec, D., Garrone, R., Zylberberg, L., Bonnaud, L., 2003. Phylogenetic analysis of vertebrate fibrillar collagen locates the position of zebrafish α3(I) and suggests an evolutionary link between collagen α chains and hox clusters. J. Mol. Evol. 57 (5), 501–514. https://doi.org/10.1007/s00239-003-2502-x.
Noble, C., Gismervik, K., Iversen, M.H., Kolarevic, J., Nilsson, J., Stien, L.H., Turnbull, J. F., 2018. Welfare indicators for farmed Atlantic salmon: tools for assessing fish welfare. https://nofima.com/publication/1636395/.
Nordberg, M., 2018. Seasonal Variation in Fillet Quality of Atlantic Salmon (*Salmo salar*). Norwegian University of Life Sciences, Ås, Norway. https://nmbu.brage.unit.no/nmbu-xmlui/handle/11250/2569081.
Nordvik, K., Kryvi, H., Totland, G.K., Grotmol, S., 2005. The salmon vertebral body develops through mineralization of two preformed tissues that are encompassed by two layers of bone. J. Anat. 206 (2), 103–114. https://doi.org/10.1111/j.1469-7580.2005.00372.x.
Patel, S.S., Molnar, M.Z., Tayek, J.A., Ix, J.H., Noori, N., Benner, D., Heymsfield, S., Kopple, J.D., Kovesdy, C.P., Kalantar-Zadeh, K., 2013. Serum creatinine as a marker of muscle mass in chronic kidney disease: results of a cross-sectional study and review of literature. J. Cachexia. Sarcopenia Muscle 4 (1), 19–29. https://doi.org/10.1007/s13539-012-0079-1.
Qian, C., Hart, B., Colombo, S.M., 2020. Re-evaluating the dietary requirement of EPA and DHA for Atlantic salmon in freshwater. Aquac. 518, 734870 https://doi.org/10.1016/j.aquaculture.2019.734870.
Roberts, R.J., Hardy, R.W., Sugiura, S.H., 2001. Screamer disease in Atlantic salmon, *Salmo salar* L., in Chile. J. Fish Dis. 24 (9), 543–549. https://doi.org/10.1046/j.1365-2761.2001.00328.x.
Sissener, N.H., Waagbø, R., Rosenlund, G., Tvenning, L., Susort, S., Lea, T.B., Oaland, Ø., Chen, L., Breck, O., 2016. Reduced n-3 long chain fatty acid levels in feed for Atlantic salmon (*Salmo salar* L.) do not reduce growth, robustness or product quality through an entire full scale commercial production cycle in seawater. Aquac. 464, 236–245. https://doi.org/10.1016/j.aquaculture.2016.06.034.
Soliman, A.S., 2018. The growth cartilage and beyond: absence of medullary bone in silver carp ribs. Mathews J. Cytol. Histol. 2 (1). https://www.mathewsopenaccess.com/full-text/the-growth-cartilage-and-beyond-absence-of-medullary-bone-in-silver-carp-ribs.
Sullivan, M., Hammond, G., Roberts, R.J., Manchester, N.J., 2007. Spinal deformation in commercially cultured Atlantic salmon, *Salmo salar* L.: a clinical and radiological study. J. Fish Dis. 30 (12), 745–752. https://doi.org/10.1111/j.1365-2761.2007.00889.x.
Veis, D.J., O'Brien, C.A., 2023. Osteoclasts, master sculptors of bone. Annu. Rev. Pathol.: Mech. Dis. 18 (1), 257–281. https://doi.org/10.1146/annurev-pathmechdis-031521-040919.
Vielma, J., Lall, S.P., 1998. Control of phosphorus homeostasis of Atlantic salmon (*Salmo salar*) in fresh water. Fish Physiol. Biochem. 19 (1), 83–93. https://doi.org/10.1023/A:1007757321695.
Witten, P.E., Huysseune, A., Hall, B.K., 2010. A practical approach for the identification of the many cartilaginous tissues in teleost fish. J. Appl. Ichthyol. 26 (2), 257–262. https://doi.org/10.1111/j.1439-0426.2010.01416.x.
Witten, P.E., Fjelldal, P.G., Huysseune, A., McGurk, C., Obach, A., Owen, M.A.G., 2019. Bone without minerals and its secondary mineralization in Atlantic salmon (*Salmo salar*): the recovery from phosphorus deficiency. J. Exp. Biol. 222 (3) https://doi.org/10.1242/jeb.188763.
Yoo, D.S., Cho, J.S., Chung, Y.-C., Rhee, S.-H., 2021. Defect structures of sodium and chloride co-substituted hydroxyapatite and its osseointegration capacity. J. Mater. Sci. 56 (9), 5493–5508. https://doi.org/10.1007/s10853-020-05645-9.
Ytteborg, E., Todorcevic, M., Krasnov, A., Takle, H., Kristiansen, I., Ruyter, B., 2015. Precursor cells from Atlantic salmon (*Salmo salar*) visceral fat holds the plasticity to differentiate into the osteogenic lineage. Biol. Open 4 (7), 783–791. https://doi.org/10.1242/bio.201411338.
Zaletel, I., Milosevic, N.T., Todorović, V.N., Kovacevic-Filipovic, M., Puškaš, N., 2017. Fractal and gray level co-occurrence matrix texture analysis of senescent and non-senescent deciduous teeth stem cells: A pilot study. FGNAMB 2, 1–6. https://doi.org/10.15761/FGNAMB.1000131.